Molecular Hydrophobicity at a Macroscopically Hydrophilic Surface

Jenée D. Cyran,[a,†] Michael A. Donovan,[a, †] Doris Vollmer,[a] Flavio Siro Brigiano,[b] Simone Pezzotti,[b] Daria R. Galimberti,[b] Marie-Pierre Gaigeot,[b] Mischa Bonn[a] and Ellen H.G. Backus[a,c*]

[a]Max Planck Institute for Polymer Research, Ackermannweg 10, 55128 Mainz, Germany

[b]LAMBE, Univ Evry, Université Paris-Saclay, CNRS UMR8587, 91025 Evry, France

[c]Department of Physical Chemistry, University of Vienna, Währinger Strasse 42, 1090 Vienna, Austria

[†]These authors contributed equally to this work.

[*]email: bonn@mpip-mainz.mpg.de; backus@mpip-mainz.mpg.de

Section S1. Phase-Resolved SFG Details

To extract the real and imaginary spectra, a gold-coated silica window was used for referencing and alignment purposes. The gold reference and the aqueous samples utilized the exact same Infrasil 302 silica window. The silica/water experiments were completed and then the silica window was coated with 100 nm gold with no chromium layer. The gold reference and aqueous samples were placed at the same height and position using an alignment laser and measuring the SFG signal at the same height on the CCD camera. Careful alignment is critical to ensure no phase ambiguities in the data. Following previously described methods for data analysis,(1, 2) the raw spectra are inversed Fourier transformed into the time domain, filtered for specific terms, and Fourier transformed into the frequency domain. Subsequently, the sample was divided by the reference, rendering the real and imaginary spectra. Similar to

www.pnas.org/cgi/doi/10.1073/pnas.1819000116

the CaF_2/water phase-resolved results,(3) a phase correction of -170° was applied to account for differences in the Fresnel factors and reflectivity between the silica/gold reference and the silica/water samples. Previous work used the silica/D_2O interface to rephase the silica/water SFG data.(4) However, the nonresonant SFG signal from the interference fringes were too weak in the high frequency region in our phase-resolved SFG spectrometer. Thus, the gold/silica interface was used for the reference. Knowing that the phase of quartz is ±90 degrees,(5) we compare the phase of quartz and gold to find that gold has a real nonresonant signal. The IR Fresnel factors (L_{zz}) were calculated following a procedure outlined by Zhuang, et al.,(6) where the index of refraction for interface 1 was set equal to water.(7) The refractive indices of water and silica were taken from literature.(8, 9)

To check for impurities at the interface, the output of the TOPAS was shifted to the C-H stretch region (around 2900 cm^{-1}). No signal was observed in the C-H region, indicating the samples were clean.

Section S2. Time-Resolved SFG Spectrometer

For the time resolved SFG spectrometer, a 1 kHz Ti:Sapphire amplified laser (Spectra-Physics Spitfire Pro) produces pulses centered at 800 nm, ~5 mJ in energy, and 40 fs in duration. A portion of the 800 nm output is used to pump two OPAs (Light Conversion TOPAS-C). One OPA collinearly mixes the signal and idler in a DFG generation stage with a $AgGaS_2$ crystal centered at roughly 3600 cm^{-1}. The Idler field from the other OPA is doubled in a BBO crystal and mixed in a KTP crystal with 2 mJ of the 800 nm beam. The output pulses, referred to as the pump, are centered around 3650 cm^{-1}. The remaining 800 nm pulse output is used as the visible upconversion pulse and is narrowed to 20 cm^{-1} by a Fabry Perot etalon. The visible, probe and excitation pulses have incident angles of 71°, 55° and 42° with

respect to the surface normal and energies of 12, 0.5, and 10 μJ per pulse at the sample, respectively. The SFG signal is divided into two signals; a signal with excitation pulse and without excitation pulse, via a vibrating galvano-mirror set to 500 Hz and synchronized to a mechanical chopper to block every other excitation pulse. The excited and not excited signals are dispersed in a spectrometer (Acton SP-300i, Princeton Instruments) and measured simultaneously on a CCD detector (Newton 971, Andor). The spectra were measured at 55 time delays ranging from -5 to 100 ps. The SFG signals are acquired for 20 s for *p*- and *s*-pump polarizations at each time delay. The results are an average of 25 scans. The visible and the probe pulses are set to *p*-polarized.

A gold coated hemisphere was used for referencing and alignment purposes. The laser beams were overlapped spatially in the center of the hemisphere, which was confirmed using a white light microscope (InfiniTube). The sample cell consisted of a custom-made glass cell sealed with a Kalrez O-ring and the Infrasil silica hemisphere placed on top.

Section S3. Contact Angle Measurements

Contact angles were measured using a DataPhysics OCA35 contact angle goniometer. Initially, 1 μL drop were deposited on the Infrasil silica windows. To reduce evaporation the silica window was placed inside a homemade transparent humidity chamber, containing a small hole for the syringe. The humidity was adjusted by placing water near the window in the chamber. Afterwards, 2 μL of water were added to the drop at a velocity of 1 μL/s and the shape of the contact line was monitored during spreading. After about 20 s, the drop reached its maximum diameter. The contact angle was determined by aligning a tangent to the drop shape by hand, as illustrated in the insets in Figure S1. For comparison, the angles were determined using the supplied software as a function of time. As evaporation cannot be

completely prevented, the contact angle slowly decreased over the course of time. After about 30s, the angle decreased by 1-2°. The measurement was consecutively repeated on four spots for the nonheat-treated and the heat-treated windows. The error of the contact angle measurements was estimated to be ±2°.

Section S4. $H_2{}^{18}O$ Measurements

Experiments were completed to compare H_2O with $H_2{}^{18}O$. If the free OH signal originates from water, one would expect a shift in the spectrum, as illustrated in Figure S1. The spectra were not corrected for Fresnel factors and the change from ^{16}O to ^{18}O could change the refractive index.

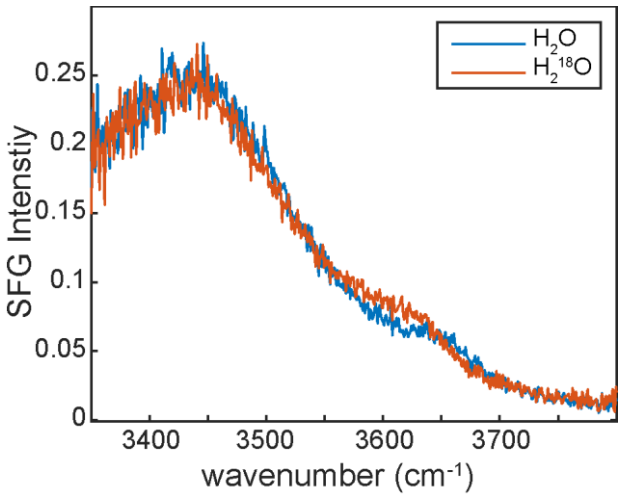

Figure S1. vSFG intensity spectra for comparison between the silica/water interface with H_2O (blue) and $H_2{}^{18}O$ (red).

Section S5. Effect of Surface Charge

The effect of surface charge was explored with a combination of intensity and phase-resolved vSFG. The intensity spectra in Figure S2a illustrate that while the hydrogen bonded water at lower frequencies changes based on pH, the high frequency peak remains constant.

The 10 mM NaCl solution has the same ionic strength as the pH 2 solution (i.e. 10^{-2} mM HCl) and was tested to verify that the ions were not contributing to the differences between the pH 2 and pH 6 spectra.

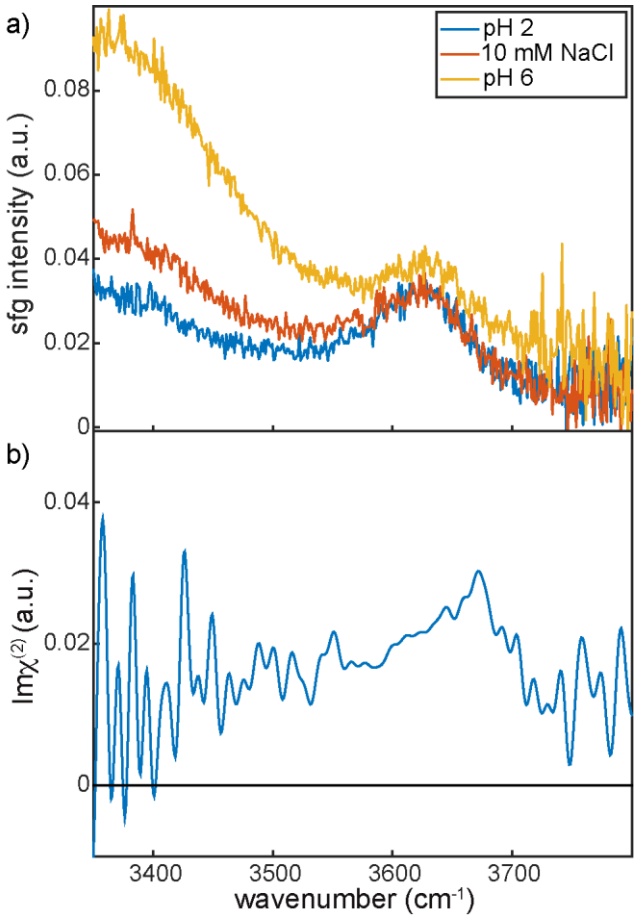

Figure S2. vSFG a) intensity spectra for pH 2, 10 mM NaCl, and ~pH 6 (MilliQ water) in contact with a silica window. b) Imaginary vSFG spectrum of pH 2 in contact with a silica window.

Figure S2b depicts the imaginary spectrum for a pH 2 solution in contact with silica. The high frequency peak is positive, which is similar to the spectral feature for a pH 6 solution in contact with silica (see Figure 1b in manuscript).

Section S6. Amorphous models and computational methods.

DFT-MD (Density Functional Theory-based Molecular Dynamics) simulations have been carried out on amorphous silica/liquid water interfaces. Two hydrophobic silica models have been chosen, displaying a surface degree of hydroxylation respectively of 4.5 SiOH/nm^2 (i.e. eight SiOH groups in our simulation box) and 3.5 SiOH/nm^2 (six SiOH in our simulation box). These models are taken from Ugliengo *et at.*,(12) respectively with a 4.5 SiOH/nm^2 and 2.4 SiOH/nm^2 silanol coverage of the surface in contact with air. Once put in contact with water, the 4.5 SiOH/nm^2 surface is found stable, while the 2.4 SiOH/nm^2 initial surface coverage evolves to 3.5 SiOH/nm^2. There is indeed a very fast adsorption of one water molecule, leading to the breaking of an adjacent siloxane bridge and subsequent dissociation of the adsorbed water molecule. This results into the creation of two new silanol groups upon local reconstruction of the silica surface, hence increasing the hydroxylation coverage of the aqueous surface from 2.4 to 3.5 SiOH/nm^2. The protonation state of these silica surfaces is around the potential of zero charge PZC (pH=2-4 conditions), and as will be seen in the next sections corresponds to isoelectric conditions (no surface electric field).

The DFT-MD simulations have been conducted with the CP2K software package,(13, 14) consisting in Born-Oppenheimer MD, BLYP(15, 16) electronic representation including Grimme D2 correction for dispersion,(17, 18) GTH pesudopotentials(19) and a combined plane waves (400 Ry energy cut-off) and SR-DZVP-MOLOPT gaussian basis set for all atoms. Dimensions of the simulation boxes are 13.386 Å X 13.286 Å X 37.0 Å (4.5 SiOH/nm^2 model) and 12.670 Å X 13.270 Å X 37.0 Å (3.5 SiOH/nm^2 model), and are periodically repeated in all directions of space. The silica slabs are 12 Å thick, composed of 204 and 198 atoms (4.5 & 3.5 SiOH/nm^2 models, respectively). Liquid water is modeled with 120 and 116 water molecules in these boxes, providing the required 1 g/cm^3 liquid density. The amorphous silica slabs were reoptimized in the gas phase at the level of theory adopted

for the dynamics, and then put in contact with bulk water. After an equilibration run of 10 ps (5 ps with possible rescaling of velocities plus 5 ps in the pure NVE ensemble) the dynamics were run in the NVE ensemble for 20 ps with a time step of 0.4 fs. All analyzed data are taken from these 20 ps thermalized trajectories.

The vSFG (vibrational Sum Frequency Generation) spectra presented in this work measure the $\chi^{(2)}(\omega)$ response in the O-H stretching region, which could arise from both the water molecules (eq 1) and from the solid surface silanols (eq 2). Surface silanols can indeed contribute to the O-H stretching signal, as shown at the quartz/water interface.(20) See next sections and main text for a description of the water layers that indeed contribute to the vSFG signals at the amorphous/water interfaces investigated here. The imaginary (and real, not presented here) parts of the resonant electric dipole nonlinear susceptibility $\chi^{(2)}(\omega)$ are calculated.

As presented in refs (21, 22), $\chi^{(2)}(\omega)$ arising from water is calculated through equation 1:

$$\chi^{(2)}_{PQR}(\omega) = \sum_{mol=1}^{M} \sum_{OH1=1}^{2} \sum_{OH2=1}^{2} \frac{i}{k_b T \omega} \int dt e^{-i\omega t} \left\langle \left(\sum_{i=1}^{3} \sum_{j=1}^{3} D_{Pi}^{mol}(t) D_{Qj}^{mol}(t) \frac{d\alpha_{ij}}{dr_{OH1}} \right) v_{OH1}^{mol}(t) \left(\sum_{k}^{3} D_{Rk}^{mol}(0) \frac{d\mu_k}{dr_{OH2}} \right) v_{OH2}^{mol}(0) \right\rangle \quad (1)$$

Similarly, the surface silanols contribution to vSFG is calculated as:

$$\chi^{(2)}_{PQR}(\omega) = \sum_{SiOH=1}^{N} \frac{i}{k_b T \omega} \int dt e^{-i\omega t} \left\langle \left(\sum_{i=1}^{3} \sum_{j=1}^{3} D_{Pi}^{SiOH}(t) D_{Qj}^{SiOH}(t) \frac{d\alpha_{ij}}{dr_{OH}} \right) v_{OH}^{SiOH}(t) \left(\sum_{k}^{3} D_{Rk}^{SiOH}(0) \frac{d\mu_k}{dr_{OH}} \right) v_{OH}^{SiOH}(0) \right\rangle \quad (2)$$

where (P,Q,R) are any x, y, z directions in the laboratory frame (here PQR=xxz & yyz for the *ssp* signal), and k_b and T are respectively the Boltzmann constant and temperature of the simulated system. $\langle \cdots \rangle$ is a time-correlation function, $d\alpha_{ij}/dr_{OH}$ and $d\mu_k/dr_{OH}$ are respectively the individual O-H bond contributions to the Raman tensor and Atomic Polar Tensor of water molecules or silanol groups. M is the number of water molecules and $OH_{1,2}$ are the two O-H oscillators/water, N is the number of silanol groups. D is the matrix that

projects the molecular frame onto the laboratory frame.

The D matrix and the projection of the velocities on the O-H bond axis ($v_{OH1,2}^{mol}$, v_{OH}^{SiOH}) are readily obtained from DFT-MD trajectories while $d\alpha_{ij}/dr_{OH}$and $d\mu_k/dr_{OH}$ terms have been parameterized. Parameterization for water is taken from ref (3, 23) as successfully applied in refs (3, 21, 22). Parameterization for silanol groups has been achieved in this work on the basis of a silicic acid building block model. Four possible Si-OH configurations have been observed along the DFT-MD trajectories of the 2 amorphous silica/water interfaces and they have thus been solely taken into account for the parameterization. The four configurations are illustrated in Figure S3: a Si-OH group donating an H-Bond to a water molecule (1), a Si-OH group accepting an H-Bond from a water molecule (2), a free Si-OH group (3) and a Si-OH group being simultaneously H-Bond acceptor and donor with water (4). Importantly, DFT-MD trajectories revealed that intra-solid H-Bonds are statistically negligible at the amorphous silica aqueous surfaces (0.2 SiOH…SiOH HBs/nm^2 for both 4.5 & 3.5 SiOH/nm^2 silanol surface coverage). Such configurations are therefore not included in the parameterization (also justifies our choice of the silicic acid building block model for parameterization).

Structures 1-4 in Figure S3 have been optimized with Gaussian09 code(24) and the computed Raman and Atomic Polar Tensor components for each of them are reported in Table S1. The final tensor elements used for the calculation of the silanols vSFG spectra in eq 2 are average weighted ($w_{1\text{-}4}$ in Table S2) according to the probability of occurrence of each of the 1-4 model configurations in the DFT-MD simulations of the amorphous silica/water interfaces.

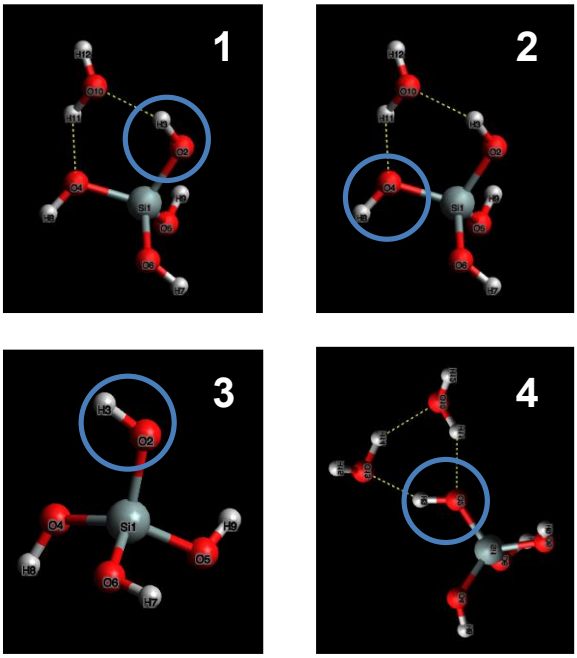

Figure S3. Illustration of the four reference model configurations used for the parameterization of the $d\mu_k/dr_{OH}$ and $d\alpha_{ij}/dr_{OH}$ terms needed in eq 2 for the vSFG theoretical spectrum of Si-OH silanol groups at aqueous amorphous silica surfaces.

Table S1. Calculated $d\mu_k/dr_{OH}$ and $d\alpha_{ij}/dr_{OH}$ terms for each of the 1-4 reference configurations presented in figure S1.

	$d\mu_x/dr_{OH}$ (D/Å)	$d\mu_y/dr_{OH}$ (D/Å)	$d\mu_z/dr_{OH}$ (D/Å)	$d\alpha_{xx}/dr_{OH}$ (Å²)	$d\alpha_{xy}/dr_{OH}$ (Å²)	$d\alpha_{xz}/dr_{OH}$ (Å²)	$d\alpha_{yy}/dr_{OH}$ (Å²)	$d\alpha_{yz}/dr_{OH}$ (Å²)	$d\alpha_{zz}/dr_{OH}$ (Å²)
1	0.005	0 .402	3.589	0.630	-0.105	0.118	0.388	0.296	3.351
2	0.267	-0.047	1.054	0.650	-0.054	0.499	0.338	0.222	2.694
3	-0.315	-0.0469	1.028	0.616	-0.0142	-0.669	0.302	0.118	2.643
4	-1.676	0.389	4.309	1.168	-0.247	-1.331	0.319	0.281	3.444

Table S2. Weights ($\mathbf{w_{1\text{-}4}}$) used to average the $d\mu_k/dr_{OH}$ and $d\alpha_{ij}/dr_{OH}$ parameterized terms from Table S1 ($\sum_i \omega_i = 1$). The weights correspond to the probability of occurrence of each model configuration in the DFT-MD trajectories of the two amorphous silica/water interfaces performed here.

	w_1	w_2	w_3	w_4
4.5 SiOH/nm²	0.63	0.02	0.00	0.35
3.5 SiOH/nm²	0.59	0.01	0.00	0.40

Section S7. Definition of interfacial layers at silica/water interfaces from DFT-MD simulations.

A critical issue in calculating and interpreting vSFG non-linear spectra is a clear and unambiguous definition of the water participating to the non-centrosymmetric spectral activity. The pioneering work of Tian and Shen(25) has laid out the principles of three universal water layers, respectively named BIL (Binding Interfacial Layer), DL (Diffuse Layer) and Bulk, that have to be considered in vSFG spectroscopy. In refs (21, 22), we have laid out and applied the formal definitions of these layers based solely on structural properties of water. This methodology has been applied here for the two investigated amorphous silica/water interfaces. Because these interfaces are at the isoelectric point, there is no DL (no surface electric field creating a DL), such that the interfacial layer is composed of the BIL only, which is therefore the only layer being vSFG active at these aqueous silica interfaces. The vSFG spectra calculated at the aqueous amorphous silica/water interfaces investigated here thus measure the O-H stretching $\chi_{ssp}^{(2)}(\omega)$ response of the solid surface silanols and of the water molecules belonging to the BIL within a rather small 3Å thickness (extracted from the definition of the water layers). Beyond the 3Å thickness of the non-centrosymmetric BIL, centrosymmetric non-SFG active bulk water is recovered. See Figure S4 for a schematic representation of the water layers at the two amorphous silica/water interfaces investigated here.

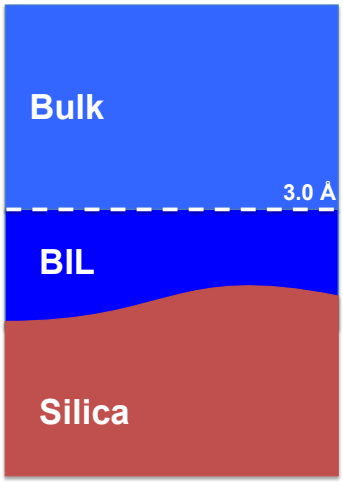

Figure S4. Schematic representations of the different water layers (BIL and Bulk) identified for the two amorphous silica/water interfaces investigated here. The 3Å thickness of the interfacial region, consisting of the BIL only, is highlighted in dark blue.

Section S8. Deconvolution of the water vSFG signal into identified water population contributions.

Water populations can be further identified in the BIL and their individual contribution to the vSFG spectra can be calculated by selecting the cartesian coordinates of the atoms belonging to a specific water population into the summation in eq. 1. To assign the BIL interfacial water molecules into one of these populations, the 20 ps trajectories have been cut into four pieces of 5 ps each over which vSFG spectra have been calculated, and then averaged in order to give the total signal. In each portion of the trajectory, a water molecule is assigned to one given population if it is found to be in that specific configuration over 80% of the simulation time (i.e. 4 ps over 5 ps). Four different water populations in the BIL have been identified with these criteria: **(a)** water molecules with one O-H oscillator pointing towards an in-plane silanol group (i.e. donor of H-Bond to the oxide surface), **(b)** water molecules with one O-H oscillator pointing towards a siloxane bridge (water donor to the surface), **(c)** water molecules rocking their pointing O-H in between a siloxane bridge and a silanol group, **(d)** water molecules not pointing any O-H towards the solid.

Only populations (a), (b) & (c) participate to the 3500-3800 cm^{-1} signatures. The contribution of populations a) and b) to the total Im $\chi^{(2)}_{ssp}(\omega)$ vSFG signal is presented in Figure 3 of the main text, respectively with the red and green lines (the total spectrum is in black lines). See the main text for all comments.

In Figure S5, we now also include the contribution of the rocking water molecules (dashed black lines). Not surprisingly, the rocking waters give a vSFG signature inbetween the signatures from the (a) and (b) populations (red and green dashed lines in fig S5), with a maximum around 3600 cm^{-1}.

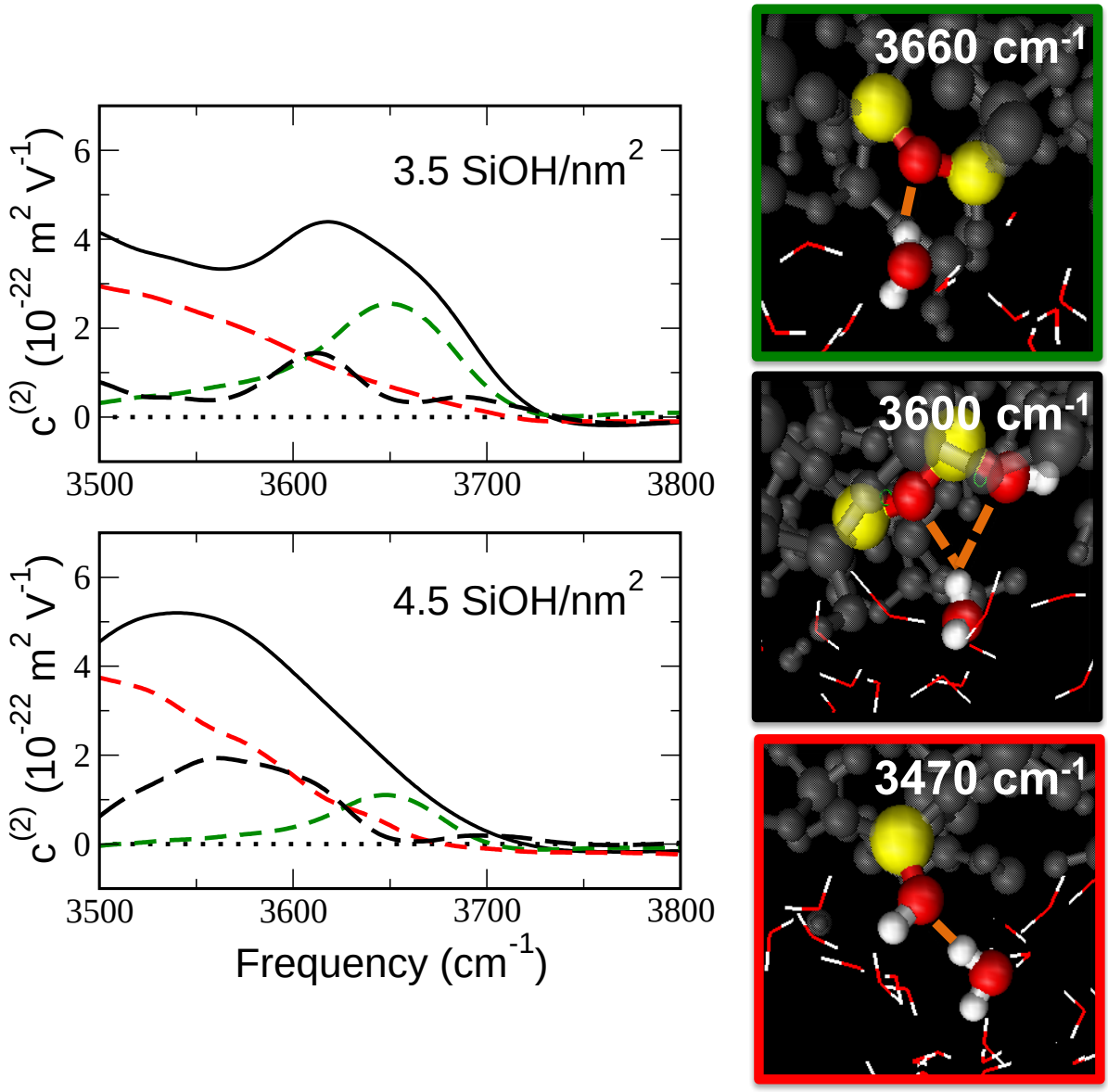

Figure S5. Left: Theoretical vSFG signal (Im $\chi_{ssp}^{(2)}$) in the 3500-3800 cm^{-1} region for two amorphous silica aqueous surfaces with various degrees of surface hydroxylation (3.5 SiOH/nm^2 and 4.5 SiOH/nm^2). The solid black line is the total vSFG signal while the dashed lines are the microscopic assignments (deconvolved signatures). Green dashed lines: water molecules that have one O-H oscillator pointing towards a siloxane bridge. Red dashed lines: water molecules with one O-H oscillator pointing towards a silanol group. Black dashed lines: rocking water molecules. **Right:** Snapshots from DFT-MD simulations illustrating the microscopic origin of the observed spectral contributions.

Section S9. Surface silanols contribution to vSFG

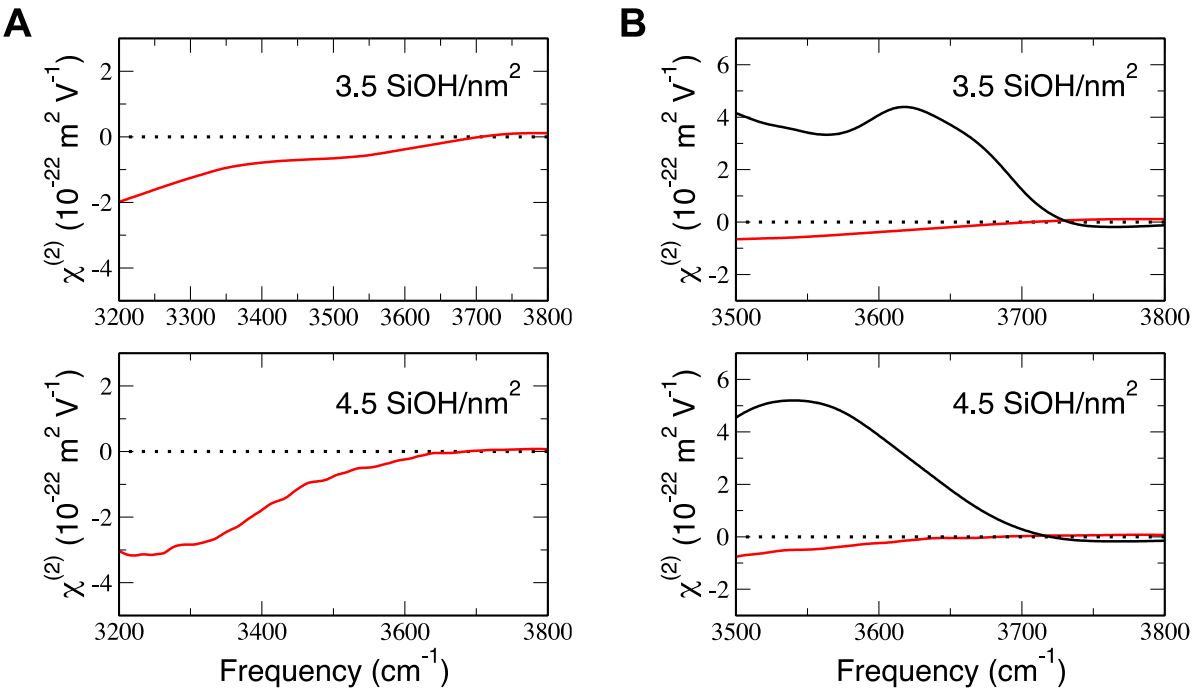

Figure S6. A: Theoretical vSFG spectral contributions ($Im\chi^{(2)}_{ssp}(\omega)$) of the surface silanol groups in the OH stretching region calculated from DFT-MD simulations for amorphous silica/water interfaces with two degrees of hydroxylation of the silica surface: 3.5 SiOH/nm^2 (left) and 4.5 SiOH/nm^2 (right). **B**: zoom in the 3500-3800 cm^{-1} spectral region of interest in the present work, where the solid contribution to vSFG (red line) is reported together with the water contribution (black line).

There are two populations of surface silanols at the amorphous surface: 'in-plane' silanols oriented parallel to the surface (13%/17% of silanols at the 4.5/3.5 SiOH/nm^2 surface coverage) and 'out-of-plane' silanols pointing out of the surface towards water (87%/83% at the 4.5/3.5 SiOH/nm^2 surface). The 'in-plane' silanols are not vSFG active due to their orientation while the 'out-of-plane' silanols donate strong H-Bonds to water, thus providing a negative band at ω<3400 cm^{-1} in the $Im\chi^{(2)}_{ssp}(\omega)$ spectra. As a consequence, the silica surface does not provide any vSFG activity in the 3500-3800 cm^{-1} spectral region of interest here.

Figure S6 presents the $Im\chi^{(2)}_{ssp}(\omega)$ vSFG contribution arising from the surface silanol groups for the two amorphous silica/water interfaces investigated here (3.5 SiOH/nm^2 *vs* 4.5

SiOH/nm^2 surface silanol coverage). The spectra clearly show that the solid does not contribute to the SFG intensity in the 3500-3800 cm^{-1} region, and instead vSFG solely arises from the interfacial water molecules identified in the 3Å thickness BIL (Binding Interfacial Layer).

Section S10. Effect of surface charge on theoretical vSFG spectra

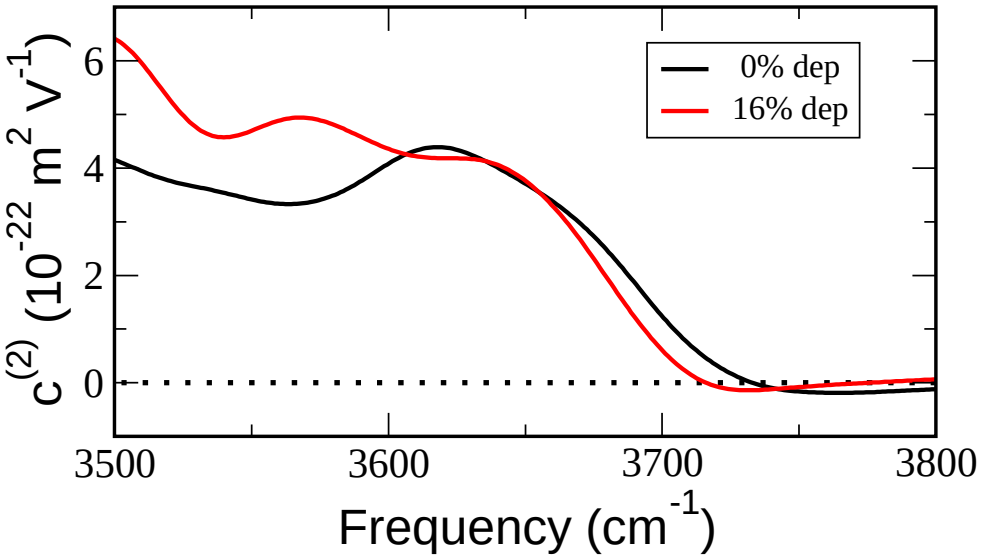

Figure S7. Theoretical vSFG signal (Im $\chi^{(2)}_{ssp}$) in the 3500-3800 cm^{-1} region for the 3.5 SiOH/nm^2 amorphous silica/water interface with 2 degrees of silica surface protonation state: fully hydroxylated surface (0% dep) and 16 % of surface sites being deprotonated (16% dep).

The effect of surface charge was explored by calculating theoretical vSFG spectra from DFT-MD simulations of the 3.5 SiOH/nm^2 amorphous silica/water interface, with the surface either fully hydroxylated or with 16 % of surface silanols being deprotonated (figure S7). The 3650 cm^{-1} band, marker of the water O-H groups pointing to siloxane bridges is observed with the same position and same intensity independently of the protonation state of the surface.

References

1. Pool RE, Versluis J, Backus EHG, Bonn M (2011) Comparative Study of Direct and Phase-Specific Vibrational Sum-Frequency Generation Spectroscopy: Advantages and Limitations. *J Phys Chem B* 115(51):15362–15369.

2. Nihonyanagi S, Yamaguchi S, Tahara T (2009) Direct evidence for orientational flip-flop of water molecules at charged interfaces: A heterodyne-detected vibrational sum frequency generation study. *J Chem Phys* 130(20):204704.

3. Khatib R, et al. (2016) Water orientation and hydrogen-bond structure at the fluorite/water interface. *Sci Rep* 6:24287.

4. Myalitsin A, Urashima S, Nihonyanagi S, Yamaguchi S, Tahara T (2016) Water Structure at the Buried Silica/Aqueous Interface Studied by Heterodyne-Detected Vibrational Sum-Frequency Generation. *J Phys Chem C* 120(17):9357–9363.

5. Sun S, et al. (2016) Phase reference in phase-sensitive sum-frequency vibrational spectroscopy. *J Chem Phys* 144(24):244711.

6. Zhuang X, Miranda PB, Kim D, Shen YR (1999) Mapping molecular orientation and conformation at interfaces by surface nonlinear optics. *Phys Rev B* 59(19):12632–12640.

7. Backus EHG, Garcia-Araez N, Bonn M, Bakker HJ (2012) On the Role of Fresnel Factors in Sum-Frequency Generation Spectroscopy of Metal–Water and Metal-Oxide–Water Interfaces. *J Phys Chem C* 116(44):23351–23361.

8. Hale GM, Querry MR (1973) Optical Constants of Water in the 200-nm to 200-μm Wavelength Region. *Appl Opt* 12(3):555–563.

9. Malitson IH (1965) Interspecimen Comparison of the Refractive Index of Fused Silica*,†. *JOSA* 55(10):1205–1209.

10. Hsieh C-S, et al. (2011) Ultrafast Reorientation of Dangling OH Groups at the Air-Water Interface Using Femtosecond Vibrational Spectroscopy. *Phys Rev Lett* 107(11):116102.

11. Xiao S, Figge F, Stirnemann G, Laage D, McGuire JA (2016) Orientational Dynamics of Water at an Extended Hydrophobic Interface. *J Am Chem Soc* 138(17):5551–5560.

12. Ugliengo P, et al. (2008) Realistic Models of Hydroxylated Amorphous Silica Surfaces and MCM-41 Mesoporous Material Simulated by Large-scale Periodic B3LYP Calculations. *Adv Mater* 20(23):4579–4583.

13. Hutter J, Iannuzzi M, Schiffmann F, VandeVondele J (2014) cp2k: atomistic simulations of condensed matter systems. *Wiley Interdiscip Rev Comput Mol Sci* 4(1):15–25.

14. VandeVondele J, et al. (2005) Quickstep: Fast and accurate density functional calculations using a mixed Gaussian and plane waves approach. *Comput Phys Commun* 167(2):103–128.

15. Becke AD (1988) Density-functional exchange-energy approximation with correct asymptotic behavior. *Phys Rev A* 38(6):3098–3100.

16. Lee C, Yang W, Parr RG (1988) Development of the Colle-Salvetti correlation-energy formula into a functional of the electron density. *Phys Rev B* 37(2):785–789.

17. Grimme S (2004) Accurate description of van der Waals complexes by density functional theory including empirical corrections. *J Comput Chem* 25(12):1463–1473.

18. Grimme S (2006) Semiempirical GGA-type density functional constructed with a long-range dispersion correction. *J Comput Chem* 27(15):1787–1799.

19. Goedecker S, Teter M, Hutter J (1996) Separable dual-space Gaussian pseudopotentials. *Phys Rev B* 54(3):1703–1710.

20. Gaigeot M-P, Sprik M, Sulpizi M (2012) Oxide/water interfaces: how the surface chemistry modifies interfacial water properties. *J Phys Condens Matter* 24(12):124106.

21. Pezzotti S, Galimberti DR, Shen YR, Gaigeot M-P (2018) Structural definition of the BIL and DL: a new universal methodology to rationalize non-linear $\chi^{(2)}$ (ω) SFG signals at charged interfaces, including $\chi^{(3)}$ (ω) contributions. *Phys Chem Chem Phys* 20(7):5190–5199.

22. Pezzotti S, Galimberti DR, Gaigeot M-P (2017) 2D H-Bond Network as the Topmost Skin to the Air–Water Interface. *J Phys Chem Lett* 8(13):3133–3141.

23. Corcelli SA, Skinner JL (2005) Infrared and Raman Line Shapes of Dilute HOD in Liquid H_2O and D_2O from 10 to 90 °C. *J Phys Chem A* 109(28):6154–6165.

24. Frisch MJ *Gaussian 09. Revision D.01*.

25. Wen Y-C, et al. (2016) Unveiling Microscopic Structures of Charged Water Interfaces by Surface-Specific Vibrational Spectroscopy. *Phys Rev Lett* 116(1):016101.